Available online at www.sciencedirect.com
ScienceDirect
Journal of Power Sources 172 (2007) 363–367
JOURNAL OF POWER SOURCES
www.elsevier.com/locate/jpowsour

Short communication

In situ diagnosis of micrometallic proton exchange membrane fuel cells using microsensors

Chi-Yuan Lee *, Guan-Wei Wu, Chi-Lieh Hsieh

Department of Mechanical Engineering, Yuan Ze Fuel Cell Center, Yuan Ze University, 135 Yuan-Tung Road, Chungli, 320 Taoyuan, Taiwan, ROC

Received 20 May 2007; received in revised form 17 July 2007; accepted 18 July 2007
Available online 24 July 2007

Abstract

This work utilizes the microsensors that are fabricated on metallic bipolar plates to measure temperature and humidity in an operating micro-proton exchange membrane fuel cell (PEMFC). Bipolar plates were constructed of stainless steel (SS-304), and the flow channel was formed on a stainless steel substrate by wet etching. The micro-temperature and humidity sensors were fabricated using micro-electro-mechanical-systems (MEMS) technology. The sensors were located on the flow channel rib.

Experimental results demonstrate that the operating temperature of fuel cell was 41.54 °C, which was measured by a micro-temperature sensor and the temperature outside the fuel cell was 37 °C, measured using a thermocouple. The gas flow rate of H_2/O_2 was 200/200 ml min^{-1} without humidification. The maximum power density of the fuel cell without and with microsensors on bipolar plates was 142 mW cm^{-2} and 56 mW cm^{-2}, respectively.

Keywords: In situ diagnosis; MEMS; Microsensors

1. Introduction

Fuel cells are a promising technology for the next generation of electrical power sources. Fuel cell power plants use an electrochemical reactor to convert chemical energy into electrical energy, and generate electricity directly from hydrocarbon fuels with a high fuel conversion efficiency and little-environmental pollution [1,2]. Fuel cells have various applications, delivering portable electricity for mobile phones, personal digital assistants (PDA), notebooks and others computer, communication and consumer electrics (3C) products. They also have mobile applications in vehicles, such as buses and ships, and stationary applications in industrial combined heat and power (CHP) and central electricity generation [3]. The use of fuel cells in portable electricity production has grown rapidly in recent years. The development of small-scale fuel cell systems will probably generate new business opportunities in the future. Miniature fuel cells require light, thin and short bipolar plates. Recent research into miniature fuel cells has led to the development of new approach that integrates micro-electro-mechanical-systems (MEMS) technology to replace traditional graphite bipolar plates [4,5]. Some investigations have studied the performance of micro-proton exchange membrane fuel cells (PEMFC) with various operational parameters, such as flow fields and operating temperature [6,7]. Miniature fuel cells that use silicon wafers as bipolar plates have been described [8]. However, silicon wafers are brittle and can easily break during fuel cell assembly. Therefore, the titanium substrate with microflow channels and a stainless steel bipolar plate, which have been utilized to reduce costs significantly are associated graphite, and have higher mechanical strength than silicon wafers [9–12].

Temperature and humidity are important parameters in the operation of a fuel cell. When the operating temperature exceeds the tolerable temperature of the membrane electrode assembly (MEA), the membrane will break. When the operating temperature of an MEA is within the tolerable range, a higher operating temperature is preferred. Mench employed a thermal sensitive resistor (thermistor) in an MEA to measure temperature [13].

* Corresponding author at: Department of Mechanical Engineering, Yuan Ze University, 135 Yuan-Tung Road, Chungli, 320 Taoyuan, Taiwan, ROC. Tel.: +886 3 4638800x2478; fax: +886 3 4558013.
E-mail address: cylee@saturn.yzu.edu.tw (C.-Y. Lee).

0378-7753/$ – see front matter © 2007 Elsevier B.V. All rights reserved.
doi:10.1016/j.jpowsour.2007.07.032

Additionally, when humidity in a fuel cell membrane is excessively high, water accumulates in the flow channel and blocks the flow of fuel into the reaction area. If humidity is excessively low, then the membrane will become dry and the performance of the fuel cell worsens. Nishikawa bored holes in a bipolar plate and applied a commercial humidity sensor to measure fuel humidity in the flow channel [14]. However, Nishikawa encountered various problems: the sensor was too large and only measured fuel humidity in the flow channel, and assembling the fuel cell was difficult.

In this investigation, MEMS technology was adopted to fabricate micro-temperature and humidity sensors on a metallic bipolar plate to measure temperature and humidity within a fuel cell.

2. Methodology and experiments

A stainless steel substrate was adopted as the material to produce metallic bipolar plates in a fuel cell. The flow channel was made by wet etching. MEMS technology was then employed to fabricate the thin film micro-temperature and humidity sensors on the flow channel rib.

2.1. The type and theory of temperature sensor

The numerous temperature sensors can be classified into two groups: contact and non-contact. Contact sensors include thermocouples and resistor sensors. Thermocouple sensors produce varying voltage signals whose leg is combined with different metals to generate a predictable voltage for a given temperature. A resistance temperature detector (RTD) yields varying resistance values that can be classified as two types: resistance wire RTDs and thermistors (thermal sensitive resistors).

A traditional thermocouple is typically adopted to measure the temperature of a fuel cell. The sensor has a large volume, so the measurement position cannot be identified precisely and fuel leaks out during fuel cell assembly. Conversely, the thin film RTD sensors have numerous advantages: its volume is small; its accuracy is high, its response time is short, and arrays can be mass-produced and placed anywhere within a fuel cell.

The resistance of a general metal is given by

$$R = \rho\frac{L}{A} \tag{1}$$

where R is resistance (Ω); ρ the resistivity (Ω-m); L the wire length (m), and A is cross-sectional area (m^2). When the temperature of an RTD varies linearly, the relationship between measured resistance and temperature change is given by

$$R_t = R_i(1 + \alpha_T \Delta T) \tag{2}$$

where R_t is resistance at t °C; R_i the resistance at i °C, and α_T is the sensitivity of the temperature sensor.

Eq. (2) can be rearranged as

$$\alpha_T = \frac{R_t - R_i}{R_i \Delta T} \tag{3}$$

where α_T is the sensitivity of the temperature sensor ($^\circ C^{-1}$) [15,16].

2.2. The theory and type of humidity sensor

Various ceramic, composite and polymer materials had been developed use in humidity sensors. Each has its own function and advantages. Polymers are attractive because they exhibit long-term stability, are sensitive to high humidity, have low manufacturing costs, are fabricated easily, and can be integrated with an integrated circuit (IC) process.

Humidity sensors that are fabricated with polymer materials are divided into resistive and capacitive types, according to their output signals. The capacitive humidity sensor is less affected by temperature than is the resistive type. A polymer typically exhibits high thermal stability and a low dielectric constant. The dielectric constant of a polymer electrolyte increases with relative humidity. The capacitance of a humidity sensor is given by

$$C = \varepsilon_0 \varepsilon(\mathrm{RH})\frac{A}{d} \tag{4}$$

where C is capacitance (F); ε_0 the dielectric constant in a vacuum; ε the dielectric constant of the environment; RH the relative humidity (%RH), A the electrode area (m^2), and d is the distance between the two electrodes (m). The sensitivity of the humidity sensor can expressed as

$$\alpha_H = \frac{\Delta C}{\Delta \%\mathrm{RH}} \tag{5}$$

where α_H is the sensitivity of the humidity sensor ($F\,\%RH^{-1}$) [15,17].

2.3. Fabrication of micro-temperature and humidity sensors

The stainless steel substrate was etched to fabricate flow channels. The micro-temperature and humidity sensors are located on the flow channel rib (Fig. 1). First, a standard RCA cleaning process was utilized to eliminate organic, oxide layers and ionic contaminants, and to evaporate Ti and spin-coated photoresist (AZ4620) onto both sides of the stainless steel substrate (Fig. 2(1)). Following photolithography to define the flow channel pattern (Fig. 2(2)), the stainless steel was etched to fabricate the flow channels using an etchant (Fig. 2(3)).

The subsequent photolithography procedure was conducted to define the bottom insulating region pattern and SiO_2 was evaporated as an insulating material. To evaporate Cr (100 Å thick) and gold (400 Å thick) in turn using an e-beam evaporator, the wet etching was adopted to generate the temperature sensor and bottom electrode of the humidity sensor (Fig. 2(4)). Polyimide was coated as a humidity-sensing film (1 μm thick) on the down electrode of the humidity sensor. A thermal evaporator deposited Ti (1500 Å thick) which was then wet-etched to produce the top electrode of the humidity sensor (Fig. 2(5)).

Finally, a photoresist was used to define the pattern as the top insulating layer following photolithography; the micro-temperature and humidity sensor were connected via Al wire

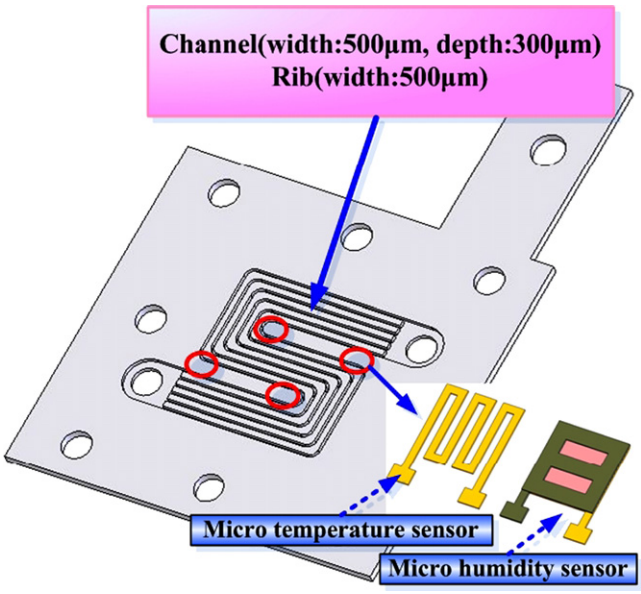

Fig. 1. Fabrication of the micro-temperature and humidity sensors on the stainless steel bipolar plate.

(Fig. 2(6)). Fig. 3 presents the flow channels on the bipolar plates following the etching of the stainless steel substrate and an optical microscopic photograph of the micro-temperature and humidity sensor.

3. Results and discussion

Stainless steel was the substrate so an insulating layer between the micro-sensors and the stainless steel was required to confirm the accuracy of the measuring signal from the temperature and humidity sensors. The selected insulation material was SiO_2 for the e-beam evaporator. SiO_2 was observed to adhere well to stainless steel at low temperature, with a low thermal conductivity, and a high resistance to erosion by organic and weak acid. Fig. 4 displays the position of the micro-temperature and humidity sensors on the flow channel rib. Results of a calibration experiment reveal that the sensitivities of the temperature and humidity sensors are $3.91 \times 10^{-3}\,^{\circ}C^{-1}$ and $0.51\,pF\,\%RH^{-1}$, respectively, and that the accuracies of the temperature and humidity sensors are less than 0.3 °C and 0.25%RH, defined for the programmable temperature and humidity chamber.

In this experiment, the standard deviation of temperature and resistance is expressed as

$$S = \sqrt{\frac{1}{n-1}\sum (x_i - \bar{x})^2} \tag{6}$$

where S denotes the standard deviation; $\sum$ refer to the sum; x_i are individual scores; $\bar{x}$ the mean of all scores, and n is the sample size (number of scores).

The correlation coefficient for temperature and resistance is

$$r = \frac{1}{n-1}\sum_{i=1}^{n}\left(\frac{x_i - \bar{x}}{s_X}\right)\left(\frac{y_i - \bar{y}}{s_Y}\right) \tag{7}$$

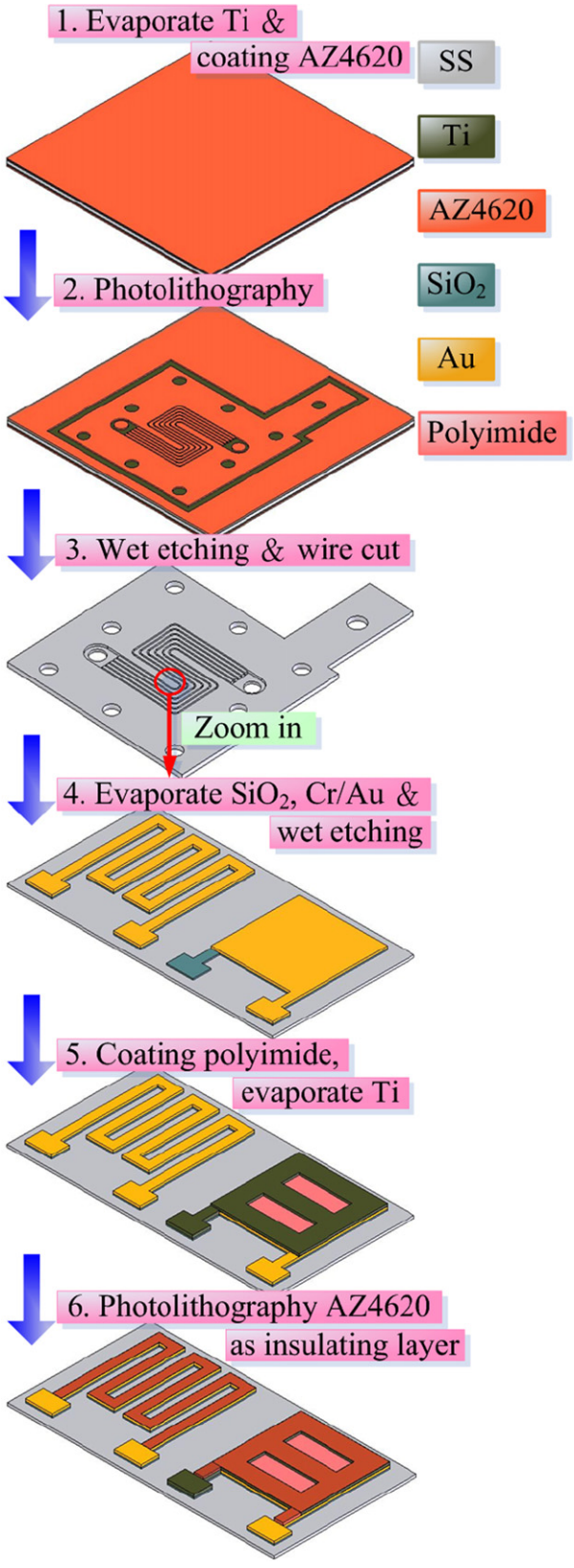

Fig. 2. Fabrication of the microflow channels and the micro-temperature and humidity sensors.

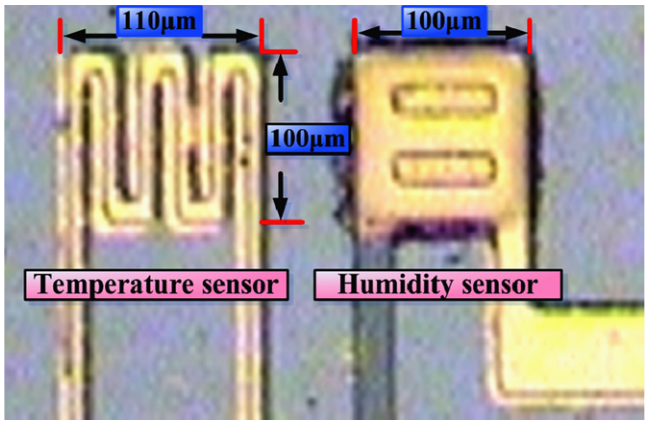

Fig. 3. Optical microscopic photograph of the micro-temperature and humidity sensor.

where r is the correlation coefficient; $\sum$ represents the sum; x_i and y_i are individual scores; $\bar{x}$ and $\bar{y}$ are the mean of all scores; s_X and s_Y are the standard deviations of x and y, and n is the sample size (number of scores) [18]. The correlation coefficient was 0.993001 approximately 1(linear); thus, the experimental results demonstrated that temperature is almost linearly correlated with resistance (Fig. 5). Fig. 6 plots the calibration curves for humidity. The sensing film accumulated steam easily at high relative humidity (>70%RH). This characteristic is intrinsic to the sensing film. Accordingly, the variation in the capacitance of the humidity sensor at higher relative humidity (70–100%RH) exceeds that at lower relative humidity (20–60 %RH). The sensitivity of the humidity sensor is 0.51 pF %RH^{-1} and the minimum measurable capacitance of the LCR meter is 0.01 pF. Therefore, even if the variation in capacitance is 0.01 nF, the LCR meter will easily measured the external change.

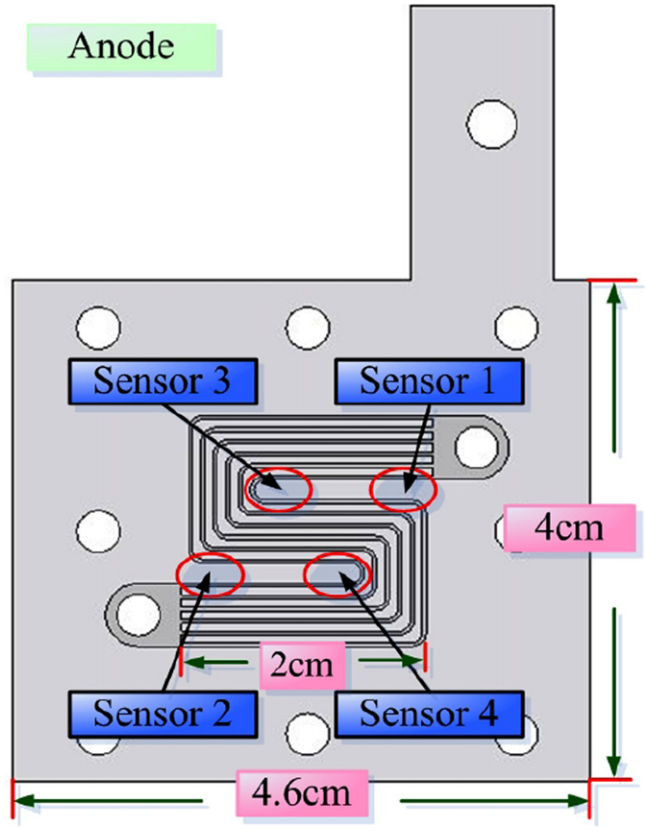

Fig. 4. Position of the micro-temperature and humidity sensors on the flow channel rib.

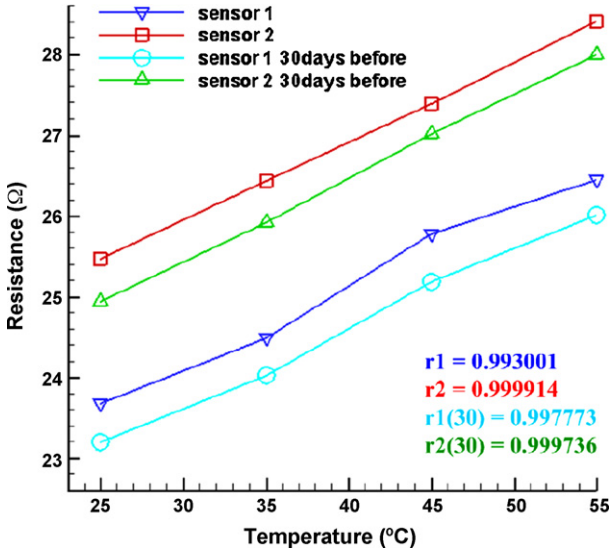

Fig. 5. Calibration curves for temperature sensors: resistance vs. temperature.

In fuel cell performance tests, the fuel cells are connected to a fuel control system; an electronic load controlled the fuel feed rate. Simultaneously, this study measured the open circuit voltage (OCV) and the output current from the fuel cell at various fuel feed rates, and measured the variation of resistance and capacitance of the temperature and humidity sensors. The operating condition of the fuel cell was 41.54 °C with an H_2/O_2 gas flow rate of 200/200 ml min^{-1} without humidification. Fabricating the micro-sensors on a flow channel rib reduced the area of electronic collection and worsened the performance of the fuel cell will from 142 mW cm^{-2} to 56 mW cm^{-2}. Figs. 7 and 8

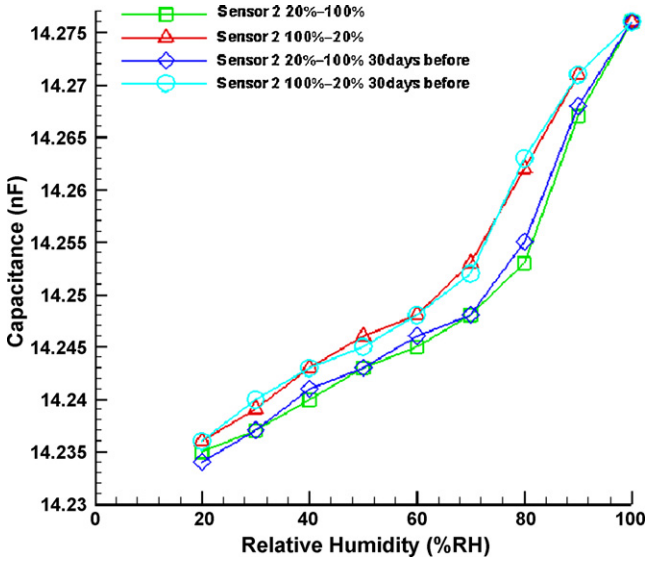

Fig. 6. Calibration curves for humidity sensors: capacitance vs. relative humidity.

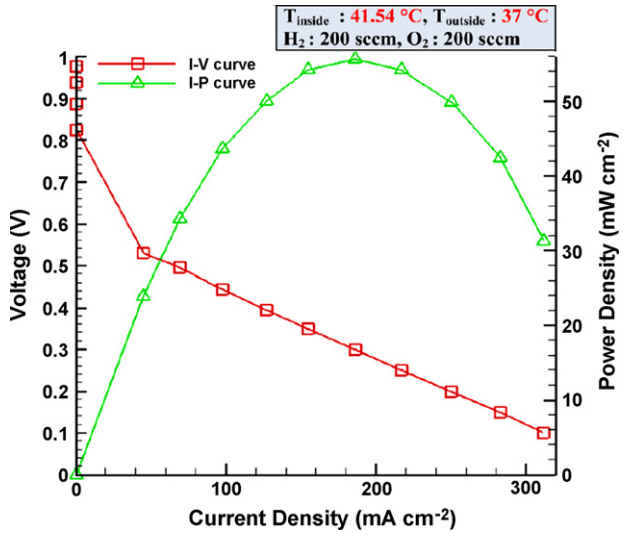

Fig. 7. Performance curves of a single cell with microsensors.

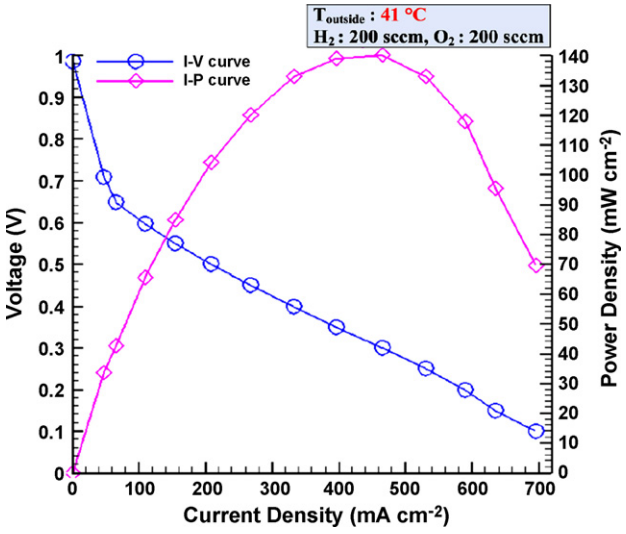

Fig. 8. Performance curves of a single cell without microsensors.

plot the performance curves of a single fuel cell with and without micro-sensors: the corresponding maximum power densities are 56 mW cm^{-2} and 142 mW cm^{-2}, respectively.

4. Conclusion

Stainless steel was wet-etched to produce a microflow channel. The micro-temperature and humidity sensors were fabricated on a microflow channel rib using the MEMS fabrication process to measure the temperature and humidity within the fuel cell. The gas flow rate of H_2/O_2 was 200/200 ml min^{-1} without humidification. The experimental results indicated that the operating temperature was 41.54 °C, measured using a micro-temperature sensor, and the temperature outside the fuel cell was 37 °C, measured using a thermocouple. The difference between temperatures gradient inside and outside the fuel cell was 4.54 °C. At a cell temperature was less than 41.54 °C, the performance increased with the temperature. The cell performance is expected to decline as temperature increases above 41.54 °C, because of dehydration.

Acknowledgements

This work was accomplished with much needed support and the authors would like to thank the financial support of this research from the aim for the top university project of Ministry of Education of R.O.C. and YZU Fuel Cell Center through the grant No. 0950026846. The authors also like to thank Professors Shuo-Jen Lee, Shih Hung Chan, Ay Su, Fangbor Weng, Guo Bin Jung of the Department of Mechanical Engineering, Yuan Ze University for their valuable advice and assistance in experiment. In addition, we would like to thank the YZU Fuel Cell Center and NTU NMES Research Center for providing access to their research facilities.

References

[1] J. Larminie, A. Dicks, Fuel Cell systems explained, 2nd ed., John Wiley & Sons, Ltd., England, 2003.
[2] X. Cheng, et al., J. Power Sources 165 (2007) 739.
[3] X. Li, Principles of Fuel Cells, Taylo & Francis, New York, 2006.
[4] S.C. Yao, et al., Energy 31 (2006) 636.
[5] S.K. Kamarudin, et al., J. Power Sources 163 (2007) 743.
[6] S.S. Hsieh, S.H. Yang, C.L. Feng, J. Power Sources 162 (2006) 262.
[7] S.S. Hsieh, et al., Energy Convers. Manage. 47 (2006) 1868.
[8] Y. Zhang, et al., Electrochem. Commun. 9 (2007) 1365.
[9] N. Wan, et al., Electrochem. Commun. 9 (2007) 511.
[10] S.J. Lee, J.J. Lai, C.H. Huang, J. Power Sources 145 (2005) 362.
[11] S.J. Lee, et al., The performance of miniature metallic PEM fuel cells, J. Power Sources 171 (2007) 148.
[12] H. Wang, J.A. Turner, J. Power Sources 128 (2004) 193.
[13] S. He, M.M. Mench, S. Tadigadap, Sens. Actuators A 125 (2006) 170.
[14] H. Nishikawa, et al., J. Power Sources 155 (2006) 213.
[15] J.S. Wilson, Sensor Technology Handbook, Butterworth-Heinemann, 2004.
[16] A.O. Hero, Foundations and applications of sensor management, Springer Verlag, 2007.
[17] C.L. Dai, Sens. Actuators B 122 (2007) 375.
[18] E.W. Weisstein, CRC concise encylopedia of mathematics, 2nd ed., Chapman & Hall/CRC, London, 2002.